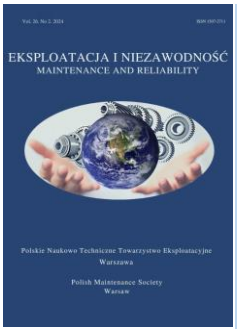

Eksploatacja i Niezawodnosc – Maintenance and Reliability

Volume 26 (2024), Issue 2

journal homepage: http://www.ein.org.pl

Article citation info:
Wan L, Niu H, Sun Z, Jiang J, Qin W, Dai H, Lubrication Reliability and Oil Churning Loss of Differential Gear Trains in a Mechanical-Hydraulic Coupling Mechanism, Eksploatacja i Niezawodnosc – Maintenance and Reliability 2024: 26(2) http://doi.org/10.17531/ein/182434

Lubrication Reliability and Oil Churning Loss of Differential Gear Trains in a Mechanical-Hydraulic Coupling Mechanism

Indexed by: Web of Science Group

Lirong Wan[a], Hao Niu[a], Zhiyuan Sun[a,*], Jinying Jiang[a], Wei Qin[a], Hanzheng Dai[b]

[a] Shandong University of Science and Technology, China
[b] Taishan University, China

Highlights

- MPS models are developed for differential gear trains.
- The influence of different factors on the lubrication reliability is analyzed.
- The height that may reduce the lubrication reliability is obtained.
- The feasibility of the MPS method is validated by experiments.

Abstract

A differential gear train (DGT) is a crucial component of a mechanical-hydraulic coupling mechanism. The transmission process generates oil churning losses, which significantly impact the overall transmission efficiency. Due to the complexity of DGTs and the unpredictability of lubrication reliability, traditional analysis of churning characteristics is inadequate. In this study, the moving particle semi-implicit (MPS) method is employed to analyze the effects of steady-state rotation speeds, dynamic rotation speeds, and oil filling heights on the oil churning characteristics of DGTs. The accuracy of the MPS method in predicting churning loss is illustrated by the Mean Absolute Percentage Error (MAPE) of 6.4% obtained experimentally. It is concluded that: increasing the oil filling height improves lubrication reliability by 20.9%, but results in greater power loss. The lubrication reliability and power loss of DGTs with different output forms are mutually advantageous under different influencing factors. This paper helps to improve the lubrication reliability of DGTs.

Keywords
differential gear train, moving particle semi-implicit, lubrication reliability, churning loss

1. Introduction

Improving the transmission efficiency of hydraulic-mechanical parallel-coupled transmission systems can significantly reduce fuel consumption, promoting energy savings and emissions reductions, and addressing global warming concerns. DGTs are a key component of these systems because they offer high efficiency and strong differential drive ability, among other benefits. However, these benefits are accompanied by challenges related to complex structure and intense movement, which can impact operational reliability and shorten the working life of component parts [29]. To address these challenges, lubrication and cooling strategies such as splash lubrication and oil spray lubrication are employed. Nevertheless, such methods bring oil churning losses and affect transmission efficiency [11,24]. Oil churning power loss is a particularly significant factor, accounting for up to 30% of the total loss [2,5,10,23], which severely affects the efficiency of gear transmission systems.

In the past, a large number of experimental studies on the

(*) Corresponding author.
E-mail addresses: L. Wan (ORCID: 0000-0002-4279-1598) lirong.wan@sdust.edu.cn, H. Niu (ORCID: 0009-0007-3013-7672) niuhao@sdust.edu.cn, Z. Sun (ORCID: 0000-0003-0557-6781) zysun@sdust.edu.cn, J. Jiang (ORCID: 0009-0007-1909-2899) jyjiang@sdust.edu.cn, W. Qin 15854430930@163.com, H. Dai (ORCID: 0000-0002-2778-4031) dhz@tsu.edu.cn,

churning power losses of gears have been carried out by international researchers. Kahraman et al. [17] developed a special testing device for planetary gear trains and found that the main sources of churning losses are the viscous friction and centrifugal force inside the planetary bearings. Hammami et al. [12,13] obtained the average friction coefficient of a meshing gear by testing the oil churning torque losses of a spur gear on an FZG test bed and established a global power loss model considering load-dependent and load-independent losses. Zhu et al. [28] conducted splash lubrication tests on single face gear, and established a physical model for calculating the load-independent loss of face gear considering the dynamic oil filling height.

Computational fluid dynamics (CFD) methods have gradually become a major tool in analyzing gear churning loss with the progress of science and technology. Among them, mesh-based finite volume analysis methods are widely used. Concli et al. [1,3,4] found that the gear oil compression power losses decrease when the temperature increases and increase when the rotation speed increases. For planet gears, when the temperature is low, the power losses decrease with the temperature at a high rate. Liu et al. [20,21,22] built an FZG gear test bed and established a 3D simulation model considering two-phase flow. By comparing the simulation results with the test results, it was found that they have good consistency. Ouyang et al. [25] investigated the jet lubrication of orthogonal face gear pair and found that a reasonable nozzle layout can improve the lubrication reliability. Hu et al. [14,15] proposed a model to estimate the oil churning power loss in a helicopter spiral bevel gear transmission gearbox and analyzed how different factors affect the lubrication reliability due to oil churning. Zeng et al. [27] analyzed the effect of tooth width and rotation speed on the lubrication reliability of gear pairs with different meshing modes and found that the difference in churning loss mainly came from the viscous force of large gears.

In recent years, some scholars have used meshless particle methods to study the oil churning characteristics of gears. Ji et al. [16] adopted the meshless smooth particle hydrodynamics (SPH) method to analyze the lubricant fluid field inside a gearbox, and compared it with the experimental results to verify the feasibility of the SPH method. Based on the SPH method, Keller et al. [18] studied the diffusion phenomenon and torque when the oil flow with different inclination angles impinges on a spur gear, and compared with the VOF simulation, it was found that the SPH method can save a lot of time. Deng et al. [7,8] used the MPS method to quantitatively analyze the effects of various factors on the oil distribution in roller-enveloped worm gear transmission and observed it through experiments. The outcomes indicated a good agreement between the MPS method and the experimental results.

Most existing research has primarily examined churning losses in a single gear or a fixed axis meshing gear pair, with limited attention given to a DGT with ring gear rotation. Consequently, systematic analysis of the dynamic flow field features and churning loss of DGTs has been challenging, a problem addressed in this paper. The structure and motion forms of DGTs are complex, and other analysis methods (such as SPH, Boundary Element Method, Finite Volume Method, Discrete Element Method) are cumbersome in pre-processing, difficult to solve, and inefficient in addressing lubrication reliability. In contrast, the MPS method offers simplicity in computation and high accuracy. Therefore, this study adopts the MPS method to explore the impact of rotational speed and initial oil injection height on the lubrication reliability and churning loss of DGTs with different output forms. Moreover, the study investigates the effect of different oil filling heights on churning characteristics under dynamic speed conditions and discusses any observed differences. Finally, experiments validate the efficacy of the MPS method.

2. MPS-based DGT model

2.1. DGT structure

To analyze the oil churning losses of DGTs more comprehensively, a differential gearbox with a planet carrier output shaft (DGPCOS) and a differential gearbox with a ring gear output shaft (DGRGOS) in [6] is taken as the research objects respectively. The mechanical-hydraulic coupling mechanism, i. e. the differential gearbox studied in this paper, mainly consists of two input shafts, a fixed axis gear pair, a sun gear, bearings, planet gears, a planet carrier, a ring gear, and a casing, as shown in Fig. 1.

The mechanical-hydraulic coupling drive system divides engine power output into two channels using a transfer gearbox. One channel transmits power to input shaft 1, while the other

channel transmits power to input shaft 2 through a hydraulic transmission unit. In the DGPCOS, input shaft 1 drives the ring gear with mechanical power flow, while input shaft 2 drives the sun gear with hydraulic power flow. The two power flows are then converged by a DGT and outputted by the planet carrier shaft. For the DGRGOS, input shaft 1 drives the planet carrier with mechanical power flow, input shaft 2 drives the sun gear with hydraulic power flow. The two power flows are then converged by the DGT and outputted by the ring gear shaft.

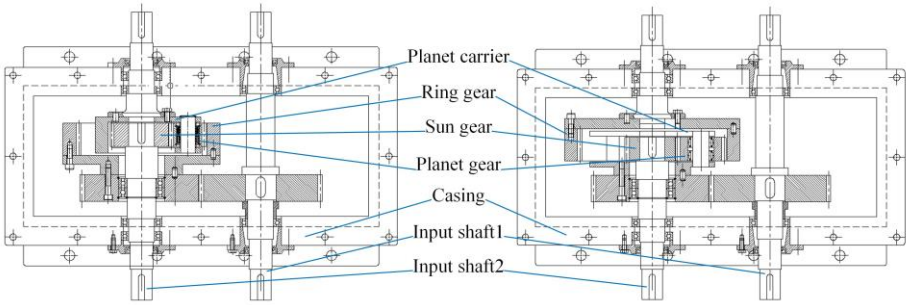

(a) (b)

Fig. 1. Different models of (a) the DGPCOS and (b) the DGRGOS.

2.2. Operating condition

The MPS method is a meshless numerical analysis method for solving incompressible fluids. It can effectively simplify the simulation processing steps, shorten the simulation time and it is easy to analyze complex kinematic boundary problems or multi-physics field problems. The basic principle of the MPS method is to replace the fluid in the computational domain with a particle swarm, to give different flow information to each fluid particle, and to solve and discretize the basic flow equations according to each interaction model based on Lagrange equations [19,26].

The MPS method takes the continuity equation (law of conservation of mass) and the Navier-Stokes equation (law of conservation of momentum) as the basic governing equations, as shown below:

$$\frac{D\rho}{Dt} = 0 \tag{1}$$

$$\frac{D\boldsymbol{u}}{Dt} = -\frac{\nabla P}{\rho} + v\nabla^2\boldsymbol{u} + \boldsymbol{g} \tag{2}$$

where $\boldsymbol{u}$ is the fluid velocity vector, t is the time, P is the pressure, ρ is the density, v is the kinematic viscosity coefficient, and $\boldsymbol{g}$ is the gravitational acceleration vector.

In the MPS method, when particles are in motion, they interact with each other through the kernel function. To improve the numerical stability and computation speed, each mathematical model uses the kernel function as the weight function to discretize the control equations [19]. Only when the distance between particles is within the effective interaction radius will they interact with each other, as shown in Fig. 2. The kernel function model is as follows:

$$w(r_p) = \begin{cases} \frac{r_e}{r_p} - 1, 0 < r_p < r_e \\ 0, r_p \geq r_e \end{cases} \tag{3}$$

where r_e is the effective radius of action of the particle and r_p is the distance between the particles.

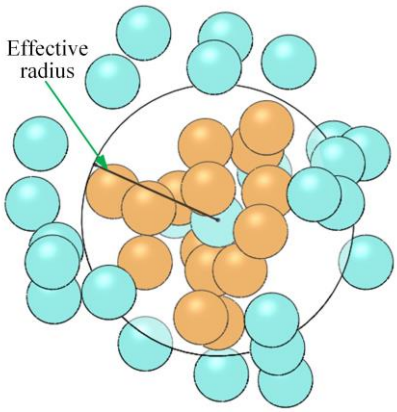

Fig. 2. Schematic diagram of particle effective radius.

The particle number density represents the combination of the function values of a particle and its neighboring particles within the range of action of the kernel function, which is a fixed value in an arrangement of particles that satisfies the incompressibility condition. The gradient model and the Laplace model are based on the kernel function discrete control equations. The expressions are as follows:

$$n = \sum_{j \neq i} w(|\boldsymbol{r_j} - \boldsymbol{r_i}|) \tag{4}$$

$$< \nabla\varphi >_i = \frac{d}{n_0} \sum_{j \neq i} \frac{\varphi_j - \varphi_i}{|\boldsymbol{r_j} - \boldsymbol{r_i}|^2} (\boldsymbol{r_j} - \boldsymbol{r_i}) w(|\boldsymbol{r_j} - \boldsymbol{r_i}|) \tag{5}$$

$$< \nabla^2 \varphi >_i = \frac{2d}{\lambda n_0} \sum_{j \neq i} \frac{\varphi_j - \varphi_i}{|\boldsymbol{r_j} - \boldsymbol{r_i}|^2} w(|\boldsymbol{r_j} - \boldsymbol{r_i}|) \quad (6)$$

where φ is the calculated particle physical parameters; d is the number of spatial dimensions, 2 for 2D and 3 for 3D; n_0 is the particle number density constant of the initial state; i, j are the particle designators; $\boldsymbol{r_j}$, $\boldsymbol{r_i}$ are the coordinate vectors of the particles; λ is the correction factor, which is calculated by the following formula:

$$\lambda = \frac{\sum_{j \neq i} w(|\boldsymbol{r_j} - \boldsymbol{r_i}|) |\boldsymbol{r_j} - \boldsymbol{r_i}|^2}{\sum_{j \neq i} w(|\boldsymbol{r_j} - \boldsymbol{r_i}|)} \quad (7)$$

Each gear is subjected to the pressure and viscous resistance of the surrounding lubricant during rotation to form a resisting moment:

$$\boldsymbol{T} = \boldsymbol{r} \times \boldsymbol{F_P} + \boldsymbol{r} \times \boldsymbol{F_v} \quad (8)$$

where $\boldsymbol{T}$ is the resistance moment vector; $\boldsymbol{r}$ is the distance vector; $\boldsymbol{F_P}$ is the pressure vector; and $\boldsymbol{F_v}$ is the viscous force vector.

Churning power loss is the product of gear churning torque loss and rotation angular velocity:

$$P_{Loss} = T_{Loss} \omega = \frac{T_{Loss} \pi n}{30} \quad (9)$$

where P_{Loss} is the churning power loss; T_{Loss} is the churning torque loss; and n is the gear rotation speed.

2.3. Simulation model

L-ckc150 lubricant is selected, its density is 812.5 kg/m^3 and kinematic viscosity is 1.5e−4 m^2/s when the temperature is 40 ℃. Considering the computer performance, the particle diameter is set to 2.5 mm, the structures of the gearboxes are set as Polygon, the pressure is set to implicit iteration model, the viscosity is set to implicit β=1 model, and the surface tension is set to Potential. To improve convergence, model simplification is performed to enhance the computational power as shown in Fig. 3, and the Courant limiter is used to prevent the computational divergence. The simulation time is set to 1 s for steady-state rotation speed and 2 s for dynamic rotation speed and the torque output interval is set to 0.01 s. As shown in Fig. 4, the oil filling height in this paper refers to the distance between the lubricant level and the center of the sun gear.

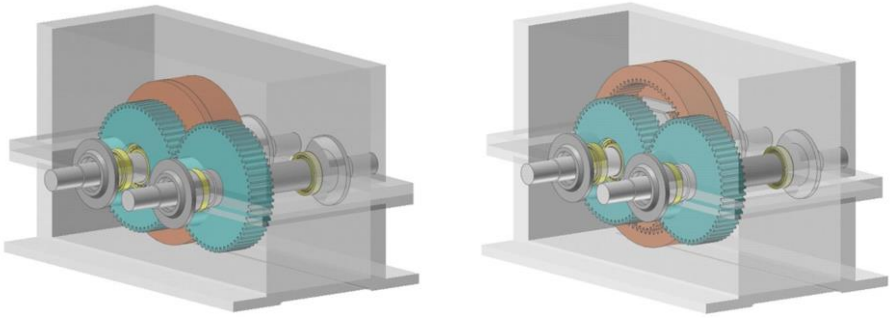

(a) (b)

Fig. 3. Simplified 3D model of (a) the DGPCOS and (b) the DGRGOS.

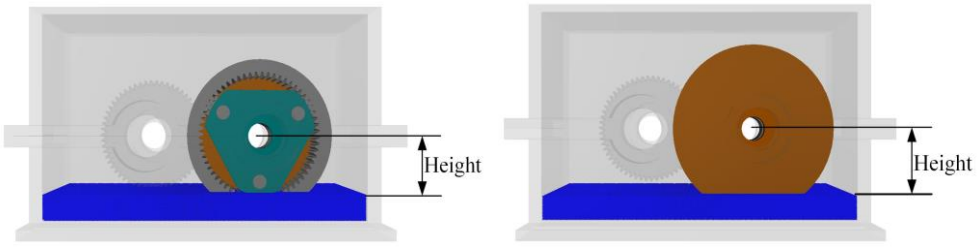

(a) (b)

Fig. 4. Schematic diagram of the oil filling height for (a) the DGPCOS and (b) the DGRGOS.

3. Analysis of fluid field features and oil churning losses of the DGPCOS

The choice of steady-state rotation speed is based on [9], which does not include analyses of dynamic rotation speed operating conditions. Given the critical role of dynamic speed in gearbox lubrication reliability, this paper explores this aspect. The "–"

only indicates the difference in the rotation direction, as shown in Table 1. The three different oiling heights are submerging the teeth of the sun gear, the center of the bottom planet gear, and the teeth of the bottom planet gear, respectively. As lubricant viscosity is temperature-dependent, considering temperature would introduce an additional variable, making it challenging to compare the simulation with the experiment when temperature changes. Therefore, the impact of temperature on lubrication reliability is not considered in this study.

Table 1. Working conditions of the DGPCOS.

Working conditions	Rotation mode	Rotation speed of sun gear (rpm)	Rotation speed of ring gear (rpm)	Rotation speed of planet carrier (rpm)	Rotation speed of planet gears (rpm)	Oil filling height (mm)
1	Steady-state rotation speed	−800	800	284.44	−1965.56	−48
2						−90
3						−112
4		−1400	1400	497.78	−3439.72	−48
5						−90
6						−112
7	Dynamic rotation speed	800 ~ −800	800	800~284.44	0 ~ −1965.56	−90
8						−112
9		1400 ~ −1400	1400	1400~497.78	0 ~ −3439.72	−90
10						−112

3.1. Fluid field features and churning losses at steady-state rotation speeds

The amount of oil in contact with the DGT is often indicative of lubrication performance, as shown in Figs. 5 and 6. Since a planet gear meshes with both the sun gear and the ring gear, the percentage of the average number of particles it contacts compared to the number of particles at full immersion can reflect the degree of lubrication reliability of the DGT. Therefore, the reliability is calculated using the planet gear initially located at the bottom as an example as shown in Fig.7. In Fig. 5, at an oil filling height of −48mm, the viscous effect causes a larger mass of splashing lubricant in the form of high-speed droplets. This increases the contact area with the DGT, ensuring reliable lubrication. At an oil filling height of −90mm, there is a decrease in oil contacting the DGT, resulting in a reduction in lubrication performance to 3.6%. At an oil filling height of −112mm, even less oil is in contact with the surface of these gears, resulting in poorer gear performance and a reliability of only 0.4%. Clearly, low oil filling heights decrease lubrication reliability and increase the risk of gear wear.

Compared with Fig. 5, Fig. 6 shows that at the same oil filling height, higher rotation speed results in greater oil agitation. The increase in rotation speed leads to higher centrifugal force, causing more oil to be thrown onto the surface of the DGT. When the oil filling height is −48 mm, the DGT easily expels oil at high speeds, but the splashed oil re-engages with it, ensuring reliable lubrication up to 15.0%, while when the oil filling height is −90 mm and −112 mm, there is less oil around the sun gear leading to reduced lubrication reliability within the DGT.

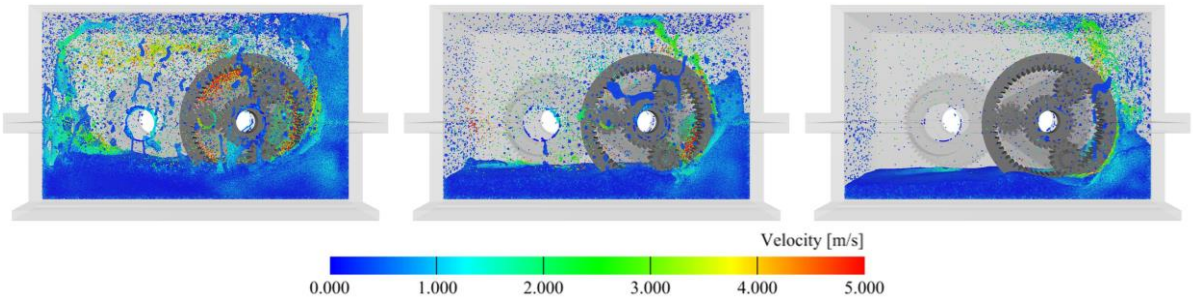

(a) (b) (c)

Fig. 5. Velocity flow field when the rotation speed of the sun gear is −800 rpm: oil filling height at (a) −48 mm, (b) −90 mm, and (c) −112 mm.

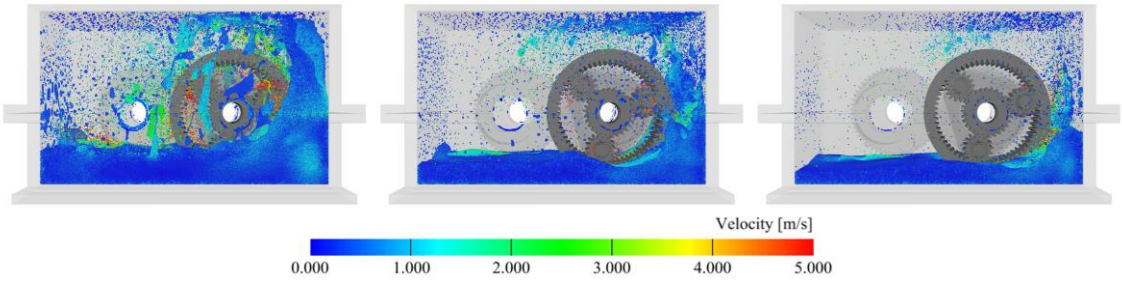

(a) (b) (c)

Fig. 6. Velocity flow field when the rotation speed of the sun gear is −1400 rpm: oil filling height at (a) −48 mm, (b) −90 mm, and (c) −112 mm.

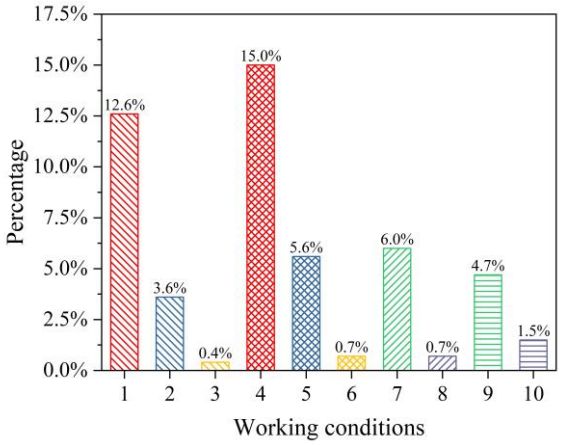

Fig. 7. Lubrication percentages of the DGPCOS.

Fig. 8 shows the variation of total churning power loss with the oil filling height and rotation speed of the sun gear, and the churning power losses of different gears in the DGPCOS for different oil filling heights at different rotation speeds of the sun gear. The total churning power loss of the DGT increases with higher oil filling height and rotation speed. Fig. 8(b) demonstrates that the power losses of the planet gears and ring gear also increase with the rise in oil filling height. The ring gear exhibits the highest percentage of power loss, followed by the planet gears, while the sun gear experiences negligible power loss (close to 0). Similar patterns are observed when the sun gear speed is −1400 rpm, with minimal churning power losses for the sun gear.

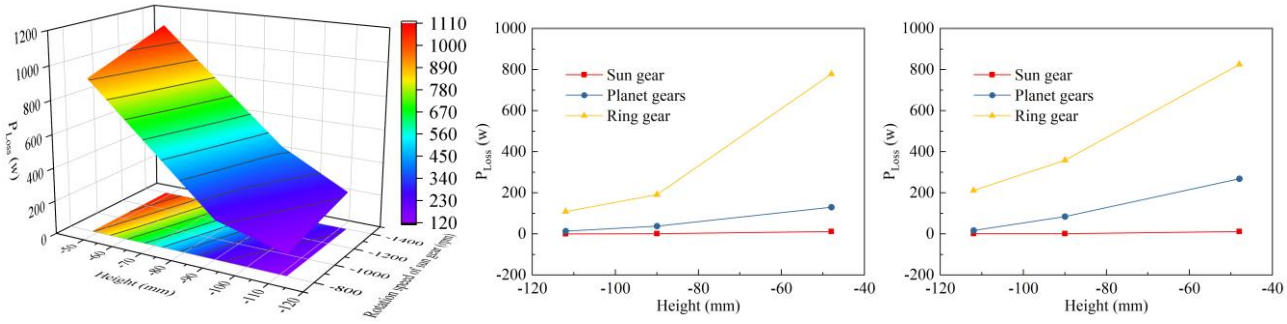

(a) (b) (c)

Fig. 8. Churning power losses of the DGPCOS: (a) the total churning power loss, (b) the churning power losses of different gears at −800 rpm, and (c) the churning power losses of different gears at −1400 rpm.

3.2. Fluid field features and churning losses at dynamic rotation speeds

The velocity fluid field of the DGPCOS under dynamic rotation speed is compared in Fig. 9 at 0.5-second intervals. For an initial oil filling height of −90 mm, decreasing carrier and sun gear speeds cause some lubricant to fall back from the casing's upper part. A second later, the sun gear rotates in the opposite direction, causing rapid expulsion of the surrounding oil. As the carrier speed decreases, the stirred oil also reduces, resulting in a rise in dynamic oil filling height that enables sufficient lubrication for the planet gears. However, when the oil filling height is −112 mm, the liquid level drops below the ring gear teeth during oil stirring on the casing's right side, leading to insufficient contact between the sun gear, planet gears, and most of the oil, thereby reducing lubrication reliability.

In Fig. 10, when the oil filling height is −90 mm, the rotation speed of the DGT is higher than in Fig. 9. This leads to an

increased oil speed within the gearbox, generating more splashed droplets due to agitation and improved lubrication reliability. However, at an extremely low oil filling height of −112 mm combined with a higher rotation speed, there is minimal oil present on the surface of the DGT. Consequently, this results in lower lubrication reliability compared to Fig. 9(b).

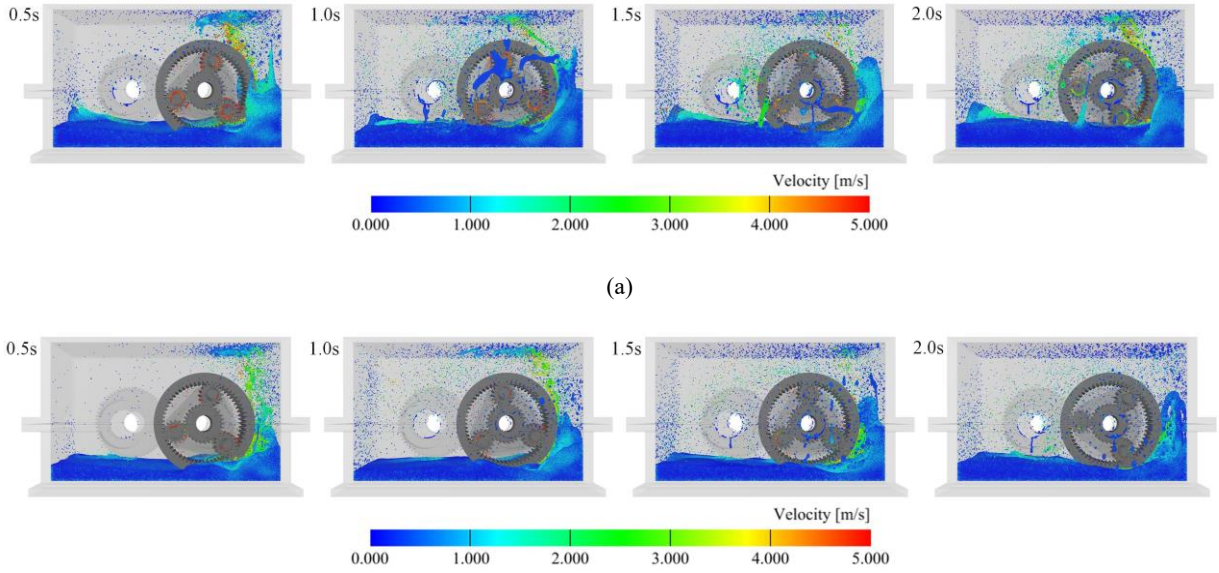

(a)

(b)

Fig. 9. Flow field distribution of the DGPCOS at different moments when the dynamic rotation speed of the sun gear is 800 ~ −800 rpm: oil filling height at (a) −90 mm and (b) −112 mm.

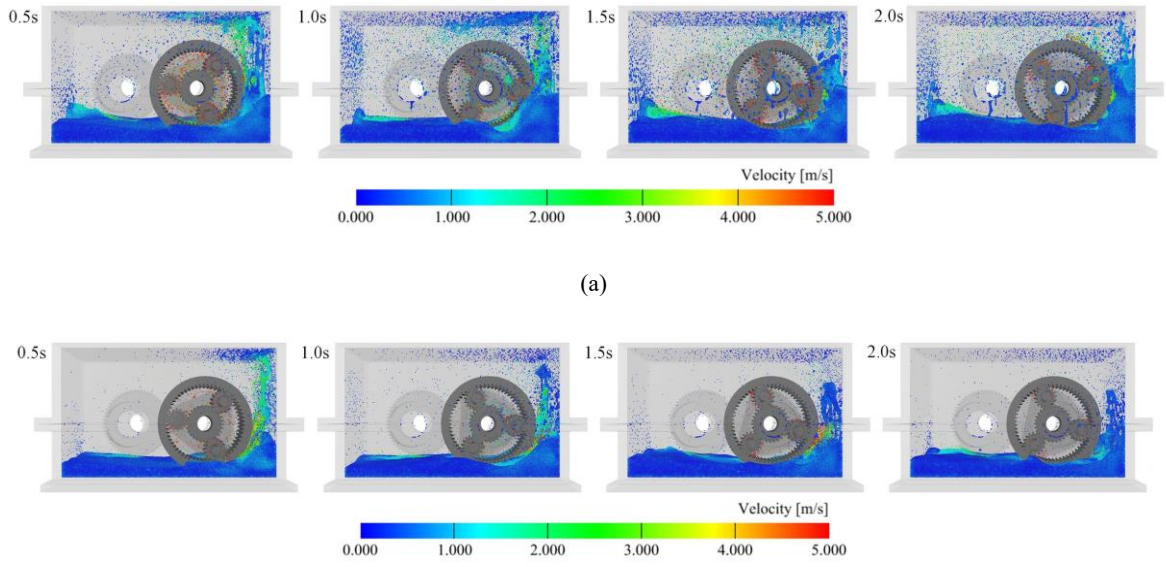

(a)

(b)

Fig. 10. Flow field distribution of the DGPCOS at different moments when the dynamic rotation speed of the sun gear is 1400 ~ −1400 rpm: oil filling height at (a) −90 mm and (b) −112 mm.

Fig. 11 shows the variation of churning torque losses and power losses at different oil filling heights with a sun gear rotation speed of 800 ~ −800 rpm. The churning torque losses of the ring gear fluctuate due to the varying exposure to oil. Additionally, dynamic changes in rotation speed notably impact the churning power loss of the planet gears, initially increasing and then decreasing within the first 1.5 seconds, followed by a subsequent rise. Variations in contact oil volume and flow field make churning torque losses unique. While all other factors remain constant, altering a single influencing factor

affects the magnitude of torque loss without significantly deviating from the curve trend. Consequently, a similar pattern is observed across different conditions. This is also reflected later.

Fig. 12 shows the variation of churning torque losses and power losses at different oil filling heights when the rotation speed of the sun gear is 1400 ~ −1400 rpm. The DGT rotates at a higher speed resulting in increased thrown oil speed, higher impact forces on oil droplets, and larger overall churning torque losses. However, the oil in contact with each gear is discontinuous droplets during rotation, leading to increased fluctuation of the churning torque losses. Compared with Figs. 11(c) and 11(d), the observation can be made that during a larger dynamic rotation speed range, there is a delay in the moment when the churning power losses of the planet gears begin to increase.

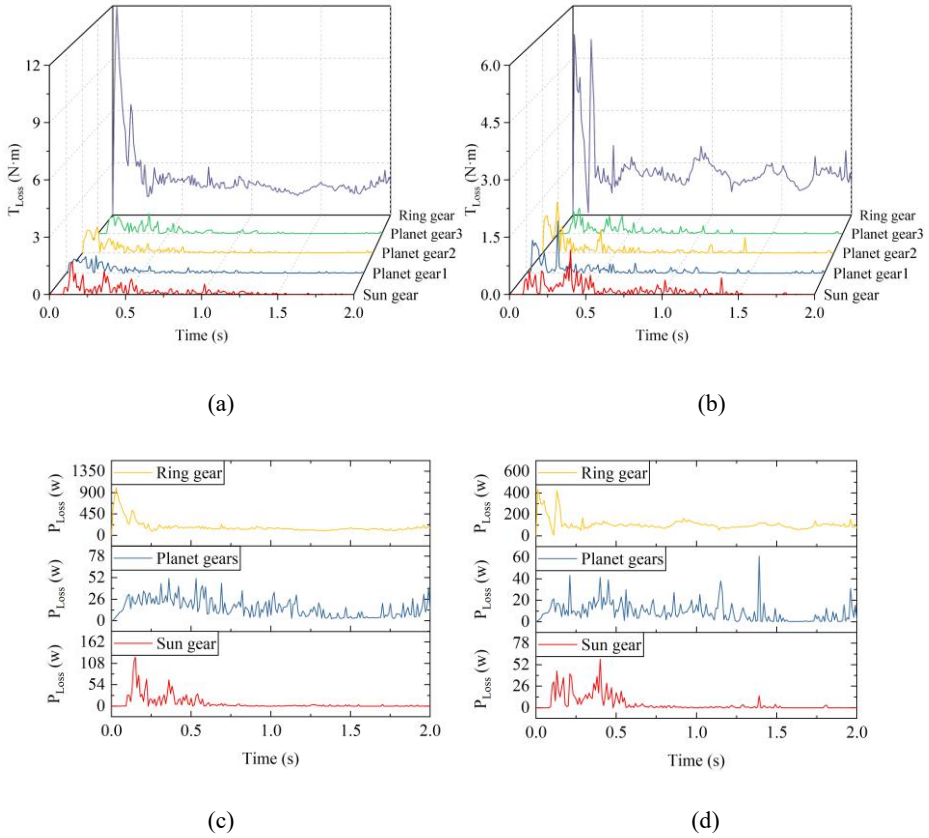

Fig. 11. Churning torque losses at (a) −90 mm, (b) −112 mm and churning power losses at (c) −90 mm, (d) −112 mm when the dynamic rotation speed of the sun gear is 800 ~ −800 rpm.

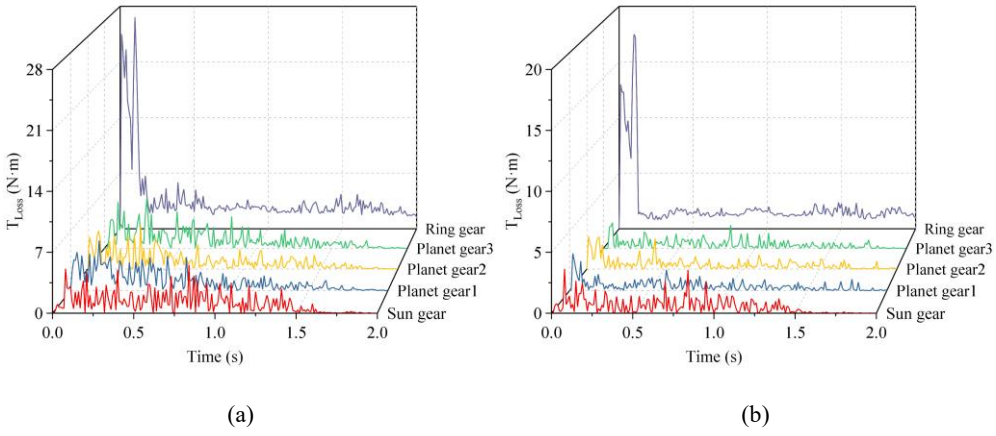

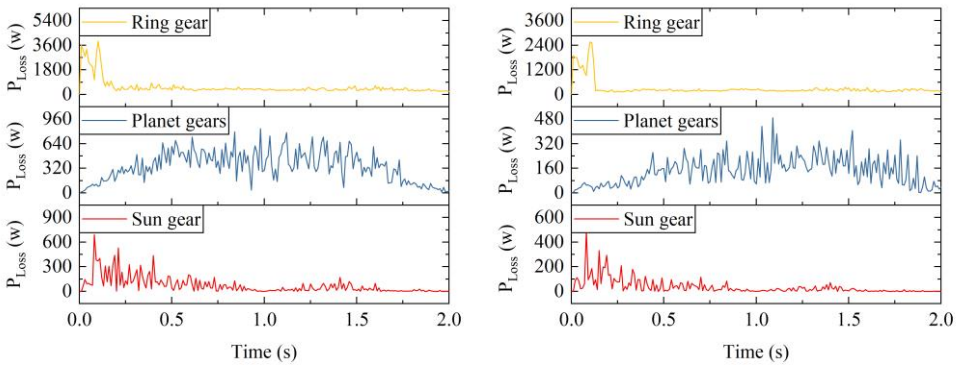

(c) (d)

Fig. 12. Churning torque losses at (a) −90 mm, (b) −112 mm and churning power losses at (c) −90 mm, (d) −112 mm when the dynamic rotation speed of the sun gear is 1400 ~ −1400 rpm.

4. Analysis of fluid field features and oil churning losses of the DGRGOS

Comparing the data in Table 1 and Table 2, it is evident that the ring speed of DGRGOS exceeds the planet carrier speed of DGPCOS, indicating that DGRGOS holds an advantage in terms of dynamic output speed. Since the dimensions of the DGRGOS are different from the DGPCOS, the oil fill heights in this section are slightly different from the previous section, but submerge the gear teeth in the same locations.

Table 2. Working conditions of the DGRGOS.

Working conditions	Rotation mode	Rotation speed of sun gear (rpm)	Rotation speed of planet carrier (rpm)	Rotation speed of ring gear (rpm)	Rotation speed of planet gears (rpm)	Oil filling height (mm)
11	Steady-state rotation speed	−800	800	1363.38	−1739.13	−40
12						−96
13						−132
14		−1400	1400	2385.92	−3043.48	−40
15						−96
16						−132
17	Dynamic rotation speed	800 ~ −800	800	800~1363.38	0 ~ −1739.13	−96
18						−132
19		1400 ~ −1400	1400	1400~2385.92	0 ~ −3043.48	−96
20						−132

4.1. Fluid field features and churning losses at steady-state rotation speeds

Figs. 13 and 14 show the velocity flow field of the DGRGOS at steady-state speeds. A higher initial oil filling height results in more oil being stirred up and better contact between gears, leading to improved lubrication reliability, as shown in Fig. 15. When the oil filling height is −40 mm, the DGT stirs up a significant amount of oil due to viscous force, resulting in more oil distribution in the DGT after dynamic equilibrium. This, along with planet gears' revolution, increases oil flow speed. The high-speed oil is more likely to splash onto the gear surfaces, allowing more oil to enter the gear mesh areas, providing a high lubrication reliability. When the oil filling height is −96 mm, the DGT is exposed to less oil, reducing reliability to 7.9%. When the oil filling height is −132 mm, the DGT stirs up minimal oil, causing a significant reduction in lubrication reliability to 1.0% and potentially causing gear teeth to wear.

At oil filling heights of −40 mm and −96 mm, Fig. 13 shows a larger volume of splashed oil, while Fig. 14 depicts a higher rotation speed of the DGT, leading to increased impact force on the oil. This results in smaller but numerous splashed droplets with higher velocity. Although the splashing speed of the oil in Fig. 13(a) is slower than that in Fig. 14(a), the droplets are sufficiently large to provide adequate lubrication to the contacted area. In Fig. 14(a), numerous small-sized droplets

with high speed and varying splashing directions enable them to contact a sufficiently large area, yielding effective lubrication. However, when the oil filling height is -132 mm, most of the thrown oil accumulates on the right side of the DGT, and the gear teeth come into contact with very little oil, with a reliability of only 1.2%.

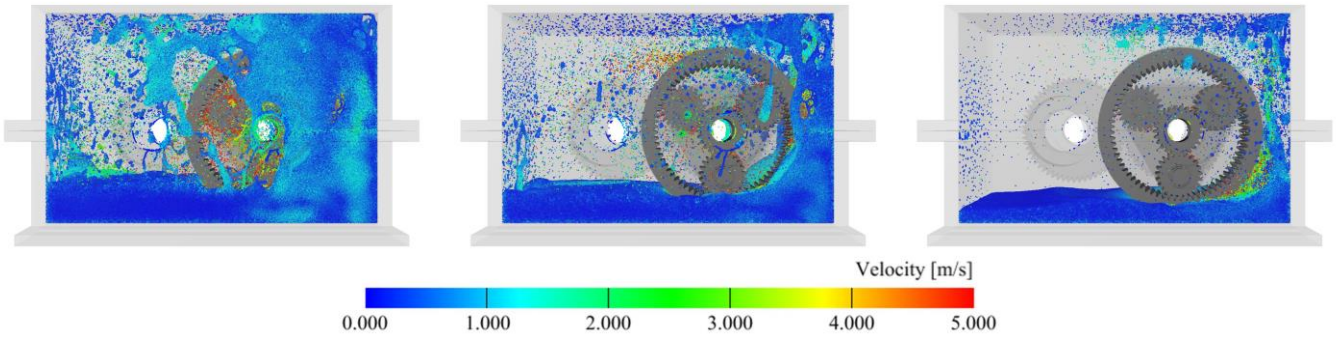

Fig. 13. Velocity flow field when the rotation speed of the sun gear is −800 rpm: oil filling height at (a) −40 mm, (b) −96 mm, and (c) −132 mm.

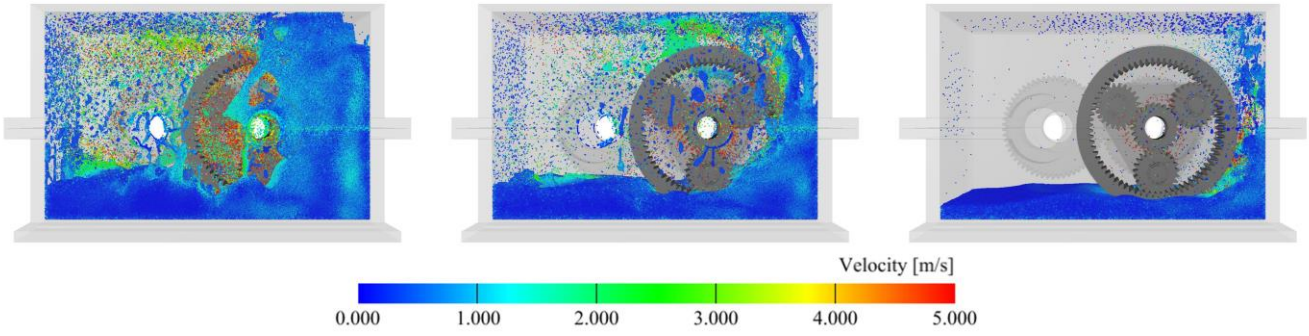

Fig. 14. Velocity flow field when the rotation speed of the sun gear is −1400 rpm: oil filling height at (a) −40 mm, (b) −96 mm, and (c) −132 mm.

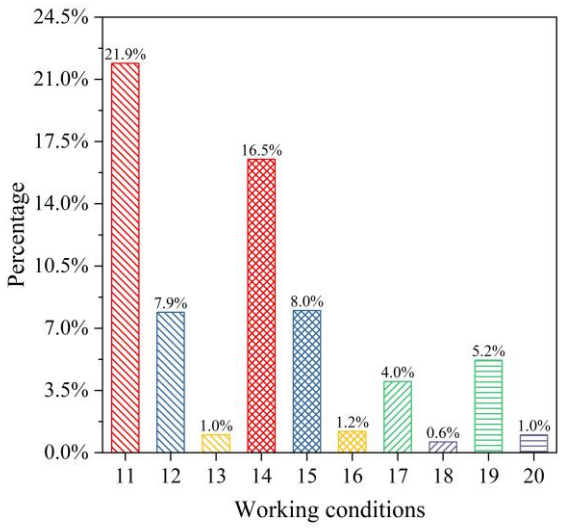

Fig. 15. Lubrication percentages of the DGRGOS.

Fig. 16(a) shows an increase in total churning power loss for the DGT with a ring gear output shaft as oil filling height and rotation speed increase. Figs. 16(b) and 16(c) further demonstrate that churning power losses of the planet gears and ring gear rise with increasing rotation speed and oil filling height. Conversely, the churning power losses of the sun gear remain minimal even at high rotation speeds due to significant oil expulsion, resulting in minimal contact with the lubricating oil and negligible churning power losses.

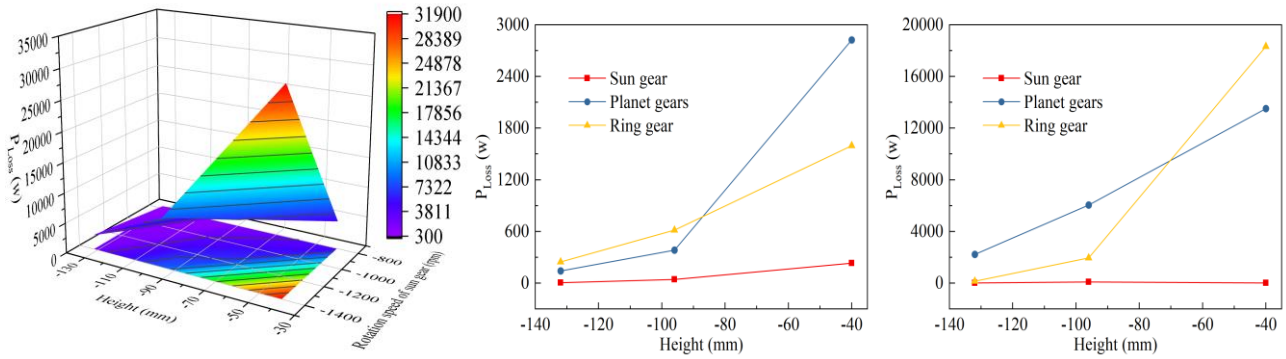

(a) (b) (c)

Fig. 16. Churning power losses of the DGRGOS: (a) the total power loss, (b) the churning power losses of different gears at −800 rpm, and (c) the churning power losses of different gears at −1400 rpm.

4.2 Fluid field features and churning losses at dynamic rotation speeds

The velocity fluid field of the DGRGOS under dynamic rotation speed is compared in Fig. 17 at 0.5-second intervals. When the oil filling height is −96 mm, significant lubricant is stirred by orbiting planet gears. At 0.5 seconds, more oil has entered gear meshing areas, and by the first second, more lubricant has reached the casing's inside top, so the lubrication reliability is high. Subsequently, as the gear ring accelerates, the splashed droplets establish consistent contact with all areas, ensuring reliable lubrication. However, when the oil filling height is -132 mm, an insufficient amount of oil reaches the sun gear and planet gears, resulting in low lubrication reliability and high risk.

In Fig. 18, the rotation speed of the DGT is higher compared to Fig. 17, resulting in a stronger impact on the oil within the casing. Consequently, the oil splashes in the form of dispersed droplets. The more high-speed oil that is splashed, the more area that is lubricated. When the oil filling height is -96 mm, the droplets at the top of the casing are small and dispersed, in contrast to Fig. 17(a) where the oil accumulates more in the same position. Similarly, when the oil filling height is -132 mm, the oil velocity near the DGT is higher than in Fig. 17(b). However, due to the low oil filling height, the lubrication reliability is compromised at both rotation speeds.

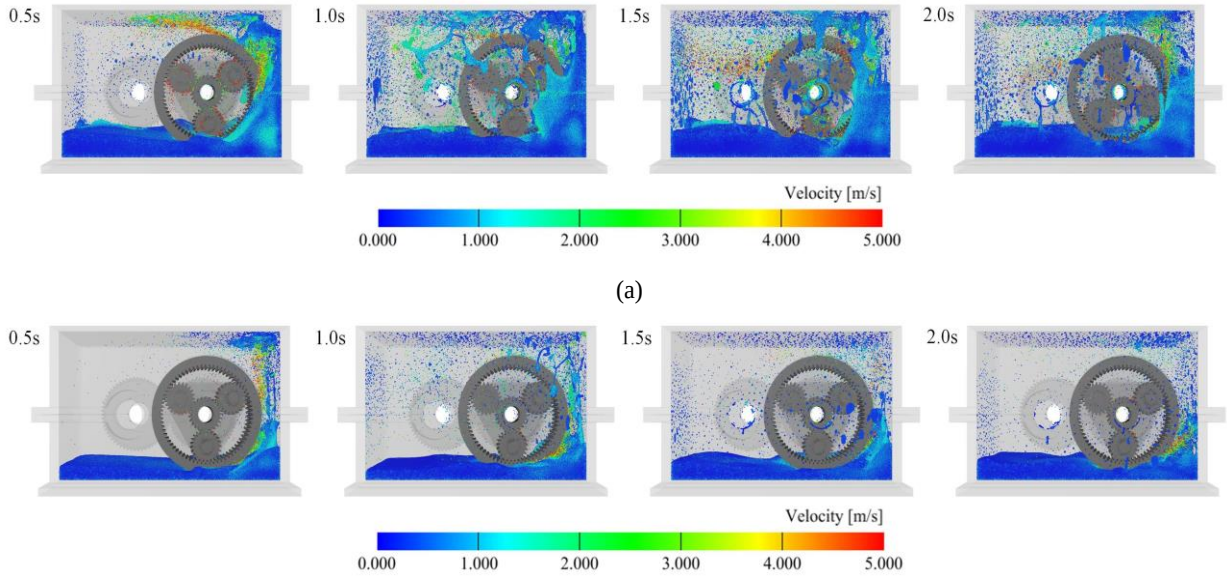

Fig. 17. Flow field distribution of the DGRGOS at different moments when the dynamic rotation speed of the sun gear is 800 ~ −800 rpm: oil filling height at (a) −96 mm and (b) −132 mm.

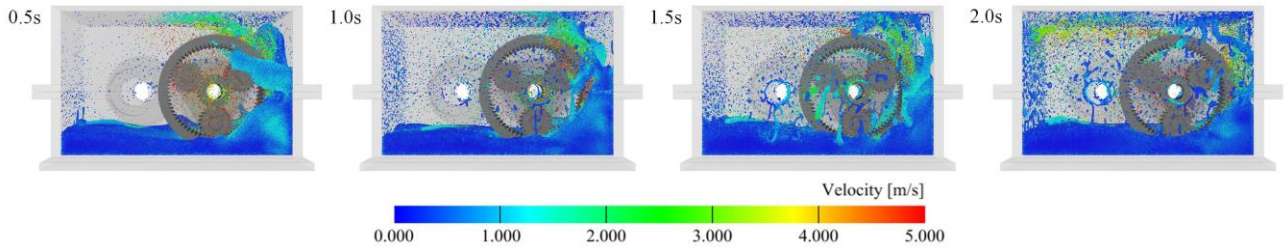

(a)

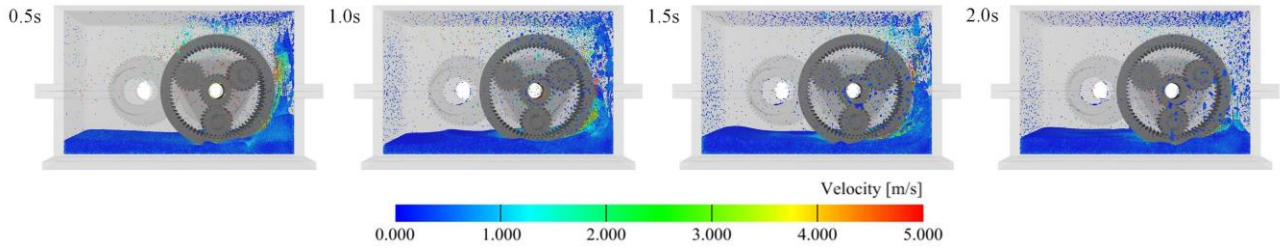

(b)

Fig. 18. Flow field distribution of the DGRGOS at different moments when the dynamic rotation speed of the sun gear is 1400 ~ −1400 rpm: oil filling height at (a) −96 mm and (b) −132 mm.

Fig. 19 shows that the churning torque losses and power losses of each gear increase with the increase of oil filling height. The sun gear experiences small churning torque losses due to minimal oil contact. In the first second, the churning power losses of the sun gear decrease as its rotation speed decreases. However, after this period, its churning power losses gradually increase with speed. The churning power losses of the planet gears increase with time because its rotation speed increases continuously. The churning power losses of the ring gear are large at the initial moment, then decrease gradually to reach a steady state, in the later stage, they fluctuate due to the increasing rotation speed.

In Fig. 20, as the dynamic speed range and oil filling height increase, the churning torque losses and power losses of each gear increase compared to Fig. 19. The churning torque losses of the planet gears first decrease with time and then gradually increase after the first second, while there is no significant change in Figs. 19(a) and 19(b). The churning power losses of the planet gears increase rapidly after 1.5 seconds, while they increase slowly in Figs. 19(a) and 19(b). The results show that, for the DGT with a ring gear output shaft, the churning power losses of planet gears increase dramatically in the later stage when the dynamic speed range is larger.

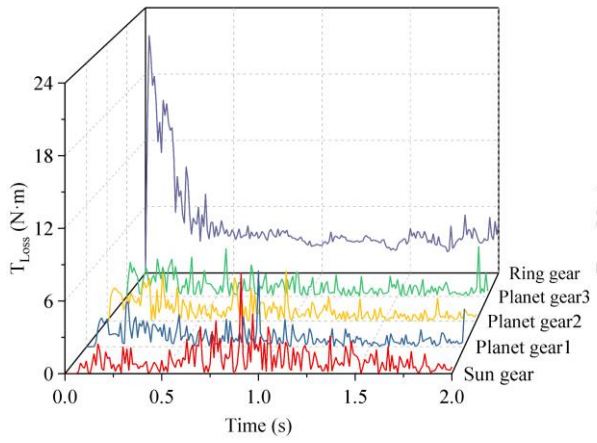

(a)

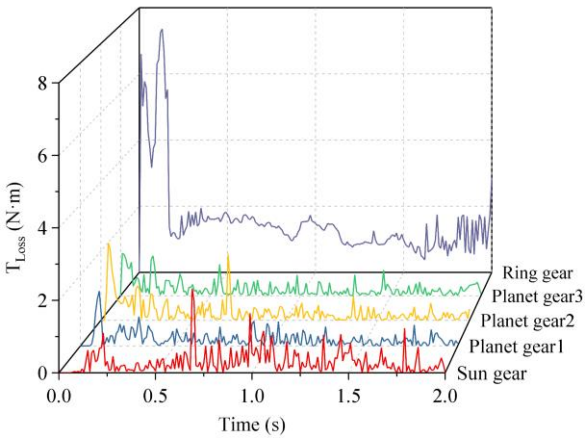

(b)

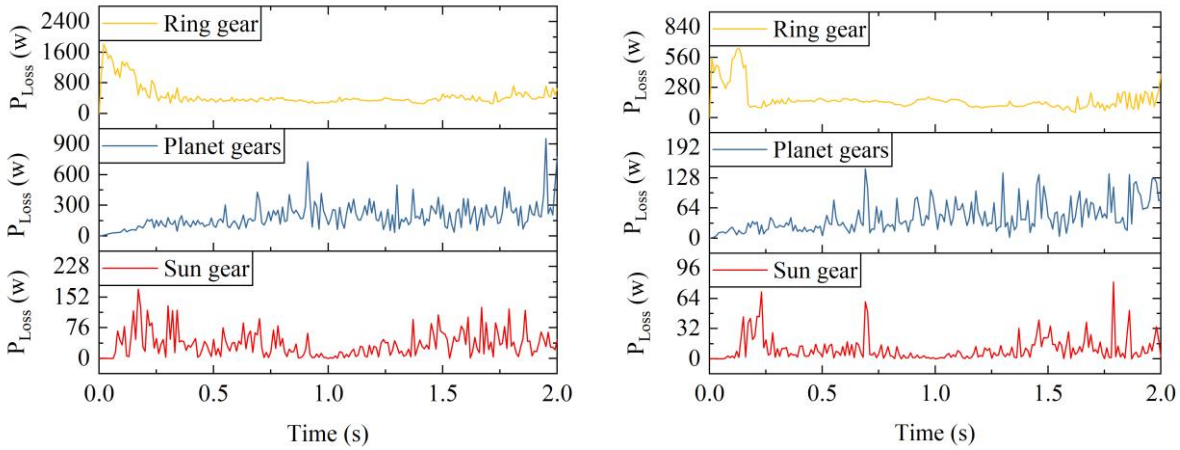

(c) (d)

Fig. 19. Churning torque losses at (a) −96 mm, (b) −132 mm and churning power losses at (c) −96 mm, (d) −132 mm when the dynamic rotation speed of the sun gear is 800 ~ −800 rpm.

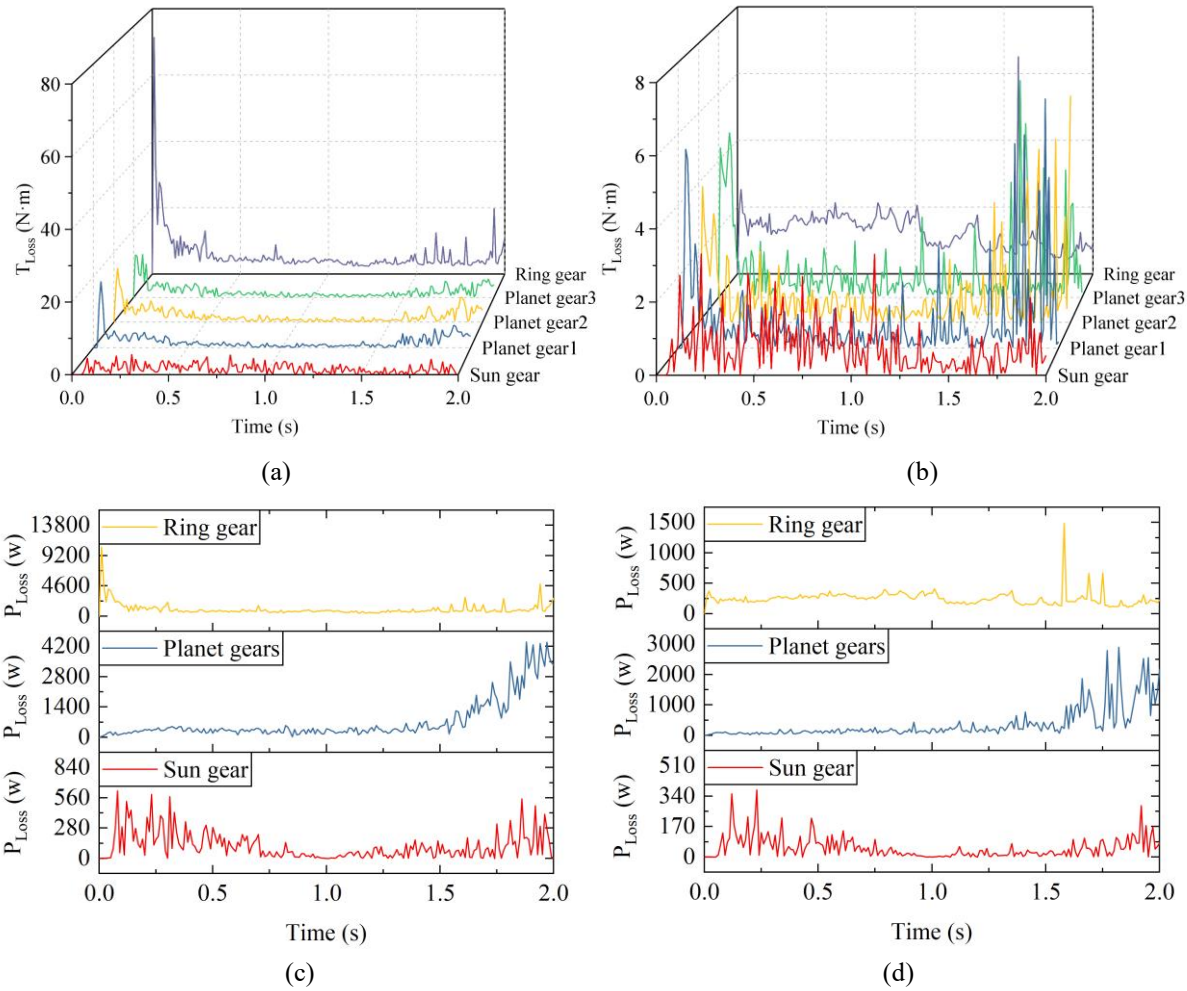

(a) (b) (c) (d)

Fig. 20. Churning torque losses at (a) −96 mm, (b) −132 mm and churning power losses at (c) −96 mm, (d) −132 mm when the dynamic rotation speed of the sun gear is 1400 ~ −1400 rpm.

5. Experimental results

Experiments were conducted on DGTs under different operating conditions to validate the accuracy of the MPS method in predicting churning loss. A test bench (Fig. 21) was built using a motor, transfer gearbox, speed-torque sensors, differential gearbox (replaceable), and dynamometer [6]. Working conditions 1-6 (Table 1) and 11-16 (Table 2) were selected for comparative tests while keeping other conditions consistent to minimize error. Power losses measured during the tests included

oil churning and friction losses from bearings, gears, and couplings. To determine churning power losses, power losses were separately measured with and without lubrication oil, and the difference was obtained as per the following equation.

$$P_{Exp} = P_{YG} - P_{NG} \quad (10)$$

where P_{Exp} is the experimental value of churning power loss, P_{YG} is the measured value of churning power loss with lubrication oil, and P_{NG} is the measured value of churning power loss without lubrication oil.

Fig. 21. Picture of the experimental setup (1) motor, (2) transfer gearbox, (3) speed-torque sensor, (4) differential gearbox, and (5) dynamometer.

Equation (9) shows that the torque loss is proportional to the power loss at the same rotation speed, so only the power loss is verified. Fig. 22 compares simulated and experimental churning power loss results for DGPCOS and DGRGOS under different operating conditions. The results show that churning power losses increase with rotation speed and oil filling height, with DGRGOS experiencing higher losses. Although some error (3.5%-17.9%) exists between the experimental and simulated values due to changes in oil temperature caused by environment temperature and gear rotation heat affecting churning losses, these errors are acceptable. The MAPE is used to quantify these errors, and the MAPE of 6.4% is sufficient to prove the validity of the simulation model. The comparison of simulation and experimental values suggests the MPS method effectively predicts churning loss, offering a reliable means of analyzing such losses in DGTs.

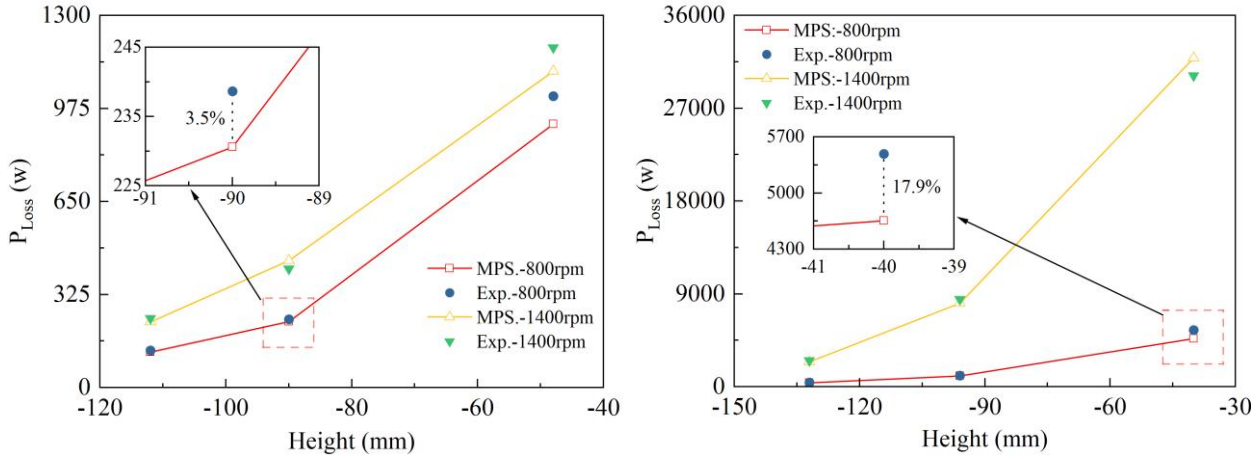

(a) (b)

Fig. 22. Comparison between experimental and MPS simulation results in terms of churning power losses of (a) the DGPCOS and (b) the DGRGOS

6. Conclusions

This paper employs the MPS method to construct simulation models of DGPCOS and DGRGOS. Experimental evidence supports the feasibility and accuracy of the MPS method in forecasting churning loss. The research delves into the impact of rotation speed and oil filling height on lubrication reliability and churning power losses of both DGTs, as well as the difference in how oil filling height affects each train's lubrication reliability and churning losses within different speed ranges. In conclusion, the study yields the following findings:

(1) Under steady-state rotation speed conditions, increasing rotation speed escalates the centrifugal force on the lubricant, resulting in higher splashing oil speeds that tend to churn the oil to the top of the casing. Meanwhile, heightening oil filling levels augments the quantity of oil in contact with the DGT during rotations, improving lubrication reliability (20.9%) and reducing wear, but wear is not quantified as it is a long-term result.

(2) The higher the rotation speed and oil filling height, the greater the impact of the oil on the gears when they rotate, resulting in higher churning torque losses and power losses. The same rule applies under dynamic speed conditions. For the DGRGOS, the churning power losses of the planet gears show a gradual increase with time in the two different speed ranges, but the increase is rapid and exponential when the dynamic rotation speed range is large.

(3) The lubrication reliability of DGRGOS can be increased by up to 9.3% compared to DGPCOS when the gears are immersed in the same position at steady-state speed, but this advantage diminishes as the oil filling height decreases.

(4) The rotation speed significantly affects the churning loss, and the dynamic output speed of DGPCOS is lower than that of DGRGOS for the same dynamic input speeds. Therefore, the DGPCOS has an advantage in churning power loss, and this advantage decreases when the oil filling height is reduced. However, higher dynamic output speeds up to 1400~2385.92 rpm can be achieved by the DGRGOS.

This work provides a feasible approach to analyzing the lubrication reliability and the churning losses of DGTs but does not consider the effects of lubricant properties and temperature on the fluid field features and churning losses of DGTs. Therefore, this is the focus of our further work to improve the comprehensive analysis of churning losses in DGTs.

Acknowledgements

This work was supposed by the National Natural Science Foundation of China (52274132) and the Shandong Construction Machinery Intelligent Equipment Innovation and Entrepreneurship Community (GTT20220206).

References

1. Concli F. Oil squeezing power losses in gears: A CFD analysis. WIT Transactions on Engineering Sciences 2012;74, https://doi.org/10.2495/AFM120041.
2. Concli F, Conrado E, Gorla C. Analysis of power losses in an industrial planetary speed reducer: Measurements and computational fluid dynamics calculations. Proceedings of the Institution of Mechanical Engineers, Part J: Journal of Engineering Tribology 2013;228(1):11-21, https://doi.org/10.1177/1350650113496980.
3. Concli F, Gorla C. Computational and experimental analysis of the churning power losses in an industrial planetary speed reducers. WIT Transactions on Engineering Sciences 2011;74, https://doi.org/10.2495/AFM120261.
4. Concli F, Gorla C. Numerical modeling of the churning power losses in planetary gearboxes: An innovative partitioning-based meshing methodology for the application of a computational effort reduction strategy to complex gearbox configurations. Lubrication Science 2017;29, https://doi.org/10.1002/ls.1380.
5. Concli F, Gorla C, Della Torre A, Montenegro G. Churning power losses of ordinary gears: A new approach based on the internal fluid dynamics simulations. Lubrication Science 2014;27:313-26, https://doi.org/10.1002/ls.1280.
6. Dai H, Wan L, Zeng Q, Lu Z, Sun Z, Liu W. Method and Test Bench for Hydro-Mechanical Continuously Variable Transmission Based on Multi-Level Test and Verification. Machines 2021;9:358, https://doi.org/10.3390/machines9120358.
7. Deng X, Wang S, Hammi Y, Qian L, Liu Y. A combined experimental and computational study of lubrication mechanism of high precision reducer adopting a worm gear drive with complicated space surface contact. Tribology International 2020;146:106261,

https://doi.org/10.1016/j.triboint.2020.106261.
8. Deng X, Wang S, Qian L, Liu Y. Simulation and experimental study of influences of shape of roller on the lubrication performance of precision speed reducer. Engineering Applications of Computational Fluid Mechanics 2020;14:1156-72, https://doi.org/10.1080/19942060.2020.1810127.
9. Diab Y, Ville F, Velex P. Investigations on power losses in high-speed gears. Proceedings of the Institution of Mechanical Engineers, Part J: Journal of Engineering Tribology. 2006;220(3):191-198. https://doi.org/10.1243/13506501JET136.
10. Guo D, Chen F, Liu J, Wang Y, Wang X. Numerical Modeling of Churning Power Loss of Gear System Based on Moving Particle Method. Tribology Transactions 2019;63:1-18, https://doi.org/10.1080/10402004.2019.1682212.
11. Guo D, Wen G, Wang Y, Luo D. A Theoretical and Experimental Study on the Power Loss of Gearbox Based on Dimensionless Analysis. Journal of Tribology. 2023;145(10), https://doi.org/10.1115/1.4062449
12. Hammami M, Feki N, Ksentini O, Hentati T, Abbes MS, Haddar M. Dynamic effects on spur gear pairs power loss lubricated with axle gear oils. Proceedings of the Institution of Mechanical Engineers, Part C: Journal of Mechanical Engineering Science 2019;234(5):1069-84, https://doi.org/10.1177/0954406219888236.
13. Hammami M, Fernandes CMCG, Martins R, Abbes MS, Haddar M, Seabra J. Torque loss in FZG-A10 gears lubricated with axle oils. Tribology International 2019;131:112-27, https://doi.org/10.1016/j.triboint.2018.10.017.
14. Hu X, Jiang Y, Luo C, Feng L, Dai Y. Churning power losses of a gearbox with spiral bevel geared transmission. Tribology International 2019;129:398-406, https://doi.org/10.1016/j.triboint.2018.08.041.
15. Hu X, Wang A, Li P, Wang J. Influence of dynamic attitudes on oil supply for bearings and churning power losses in a splash lubricated spiral bevel gearbox. Tribology International 2021;159:106951, https://doi.org/10.1016/j.triboint.2021.106951.
16. Ji Z, Stanic M, Hartono EA, Chernoray V. Numerical simulations of oil flow inside a gearbox by Smoothed Particle Hydrodynamics (SPH) method. Tribology International 2018;127:47-58, https://doi.org/10.1016/j.triboint.2018.05.034.
17. Kahraman A, Hilty DR, Singh A. An experimental investigation of spin power losses of a planetary gear set. Mechanism and Machine Theory 2015;86:48-61, https://doi.org/10.1016/j.mechmachtheory.2014.12.003.
18. Keller MC, Braun S, Wieth L, Chaussonnet G, Dauch TF, Koch R, et al. Smoothed Particle Hydrodynamics Simulation of Oil-Jet Gear Interaction1. Journal of Tribology 2019;141(7), https://doi.org/10.1115/1.4043640.
19. Koshizuka S, Oka Y. Moving-Particle Semi-Implicit Method for Fragmentation of Incompressible Fluid. Nuclear Science and Engineering - NUCL SCI ENG 1996;123:421-34, https://doi.org/10.13182/NSE96-A24205.
20. Liu H, Dangl F, Lohner T, Stahl K. Numerical Visualization of Grease Flow in a Gearbox. Chinese Journal of Mechanical Engineering 2023;36(1):28, https://doi.org/10.1186/s10033-023-00831-7.
21. Liu H, Jurkschat T, Lohner T, Stahl K. Detailed Investigations on the Oil Flow in Dip-Lubricated Gearboxes by the Finite Volume CFD Method. Lubricants 2018;6(2), https://doi.org/10.3390/lubricants6020047.
22. Liu H, Jurkschat T, Lohner T, Stahl K. Determination of oil distribution and churning power loss of gearboxes by finite volume CFD method. Tribology International 2017;109:346-54, https://doi.org/10.1016/j.triboint.2016.12.042.
23. Michaelis K, Höhn BR, Hinterstoißer M. Influence factors on gearbox power loss. Industrial Lubrication and Tribology 2011;63(1):46-55, https://doi.org/10.1108/00368791111101830.
24. Novaković B, Radovanović L, Zuber N, Radosav D, Đorđević L, Kavalić M. Analysis of the influence of hydraulic fluid quality on external gear pump performance. Eksploatacja i Niezawodność – Maintenance and Reliability. 2022;24(2):260-8, https://doi.org/10.17531/ein.2022.2.7.
25. Ouyang B, Ma F, Dai Y, Zhang Y. Numerical analysis on heat-flow-coupled temperature field for orthogonal face gears with oil–jet lubrication. Engineering Applications of Computational Fluid Mechanics 2021;15:762-80, https://doi.org/10.1080/19942060.2021.1918259.
26. Tanaka M, Cardoso R, Bahai H. Multi-resolution MPS method. Journal of Computational Physics 2018;359:106-36, https://doi.org/10.1016/j.jcp.2017.12.042.
27. Zeng Q-l, Sun Z-y, Wan L-r, Yang Y, Dai H-z, Yang Z-k. Research and Comparative Analysis of Flow Field Characteristics and Load-Independent Power Losses of Internal and External Gear Pairs. Mathematical Problems in Engineering 2020;2020:8860588,

https://doi.org/10.1155/2020/8860588.

28. Zhu X, Dai Y. Development of an analytical model to predict the churning power losses of an orthogonal face gear. Engineering Science and Technology, an International Journal 2023;41:101383, https://doi.org/10.1016/j.jestch.2023.101383.
29. Živković P, Milutinović M, Tica M, Trifković S, Čamagić I. Reliability Evaluation of Transmission Planetary Gears "bottom-up" approach. Eksploatacja i Niezawodność – Maintenance and Reliability. 2023;25(1), https://doi.org/10.17531/ein.2023.1.2.